nature biomedical engineering

SUPPLEMENTARY INFORMATION

https://doi.org/10.1038/s41551-019-0376-5

In the format provided by the authors and unedited.

High-throughput, label-free, single-cell photoacoustic microscopy of intratumoral metabolic heterogeneity

Pengfei Hai[1,2,7], Toru Imai[1,2,7], Song Xu[3], Ruiying Zhang[1], Rebecca L. Aft[4,5], Jun Zou[3*] and Lihong V. Wang[2,6*]

[1]Department of Biomedical Engineering, Washington University in St. Louis, St. Louis, MO, USA. [2]Caltech Optical Imaging Laboratory, Andrew and Peggy Cherng Department of Medical Engineering, California Institute of Technology, Pasadena, CA, USA. [3]Department of Electrical and Computer Engineering, Texas A&M University, College Station, TX, USA. [4]Department of Surgery, School of Medicine, Washington University, St. Louis, MO, USA. [5]John Cochran Veterans Hospital, St. Louis, MO, USA. [6]Caltech Optical Imaging Laboratory, Department of Electrical Engineering, California Institute of Technology, Pasadena, CA, USA. [7]These authors contributed equally: Pengfei Hai, Toru Imai. *e-mail: junzou@ece.tamu.edu; LVW@caltech.edu

Table of Contents

Supplementary Figure 1. Lateral resolution of single-cell metabolic photoacoustic microscopy (SCM-PAM).

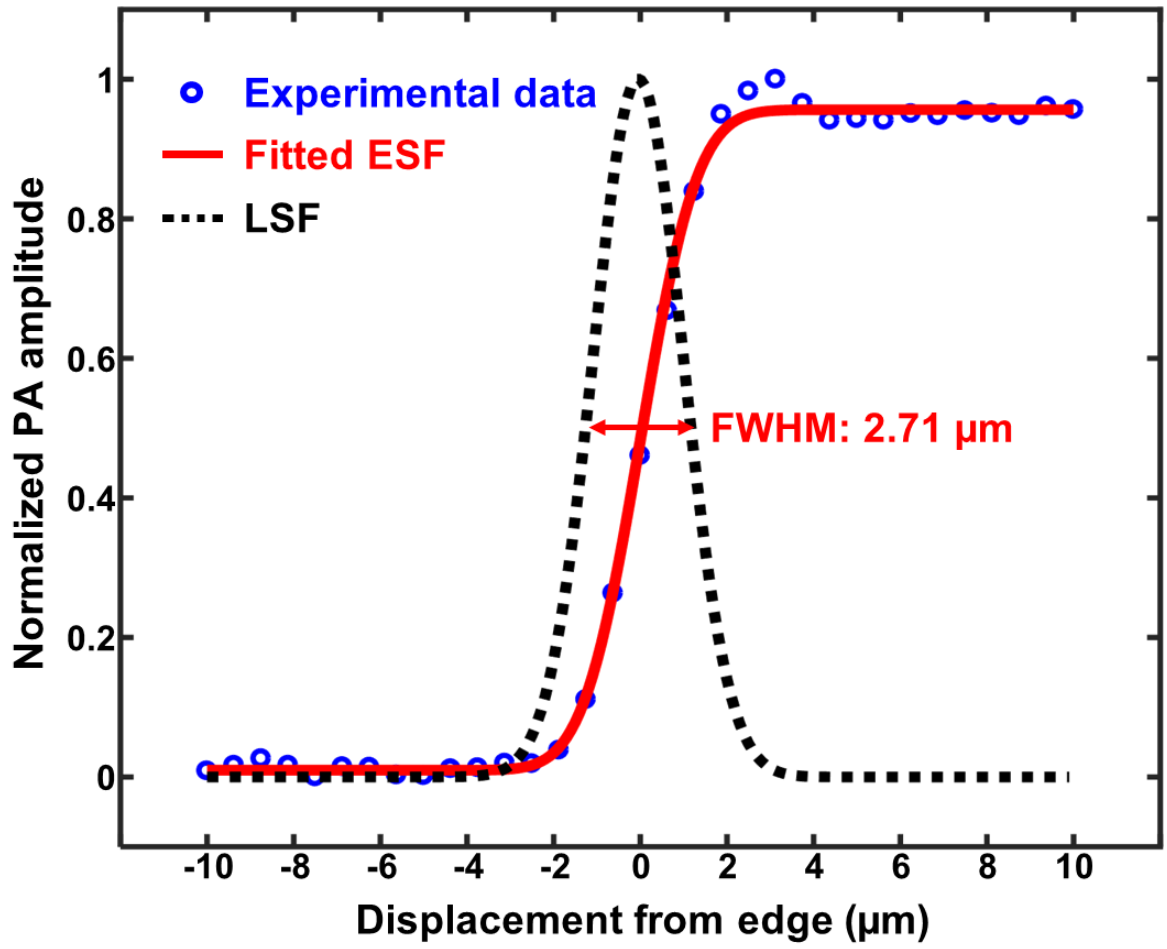

Supplementary Figure 1. Lateral resolution of single-cell metabolic photoacoustic microscopy (SCM-PAM). The measured data (blue circles) were fitted to deduce an edge spread function (ESF, red solid line). The line spread function (LSF, black dotted line) was calculated by differentiating the fitted ESF. The lateral resolution was quantified as the full width at half maximum (FWHM) of the LSF.

Supplementary Figure 2. Fabrication and operation of the high-density microwell array.

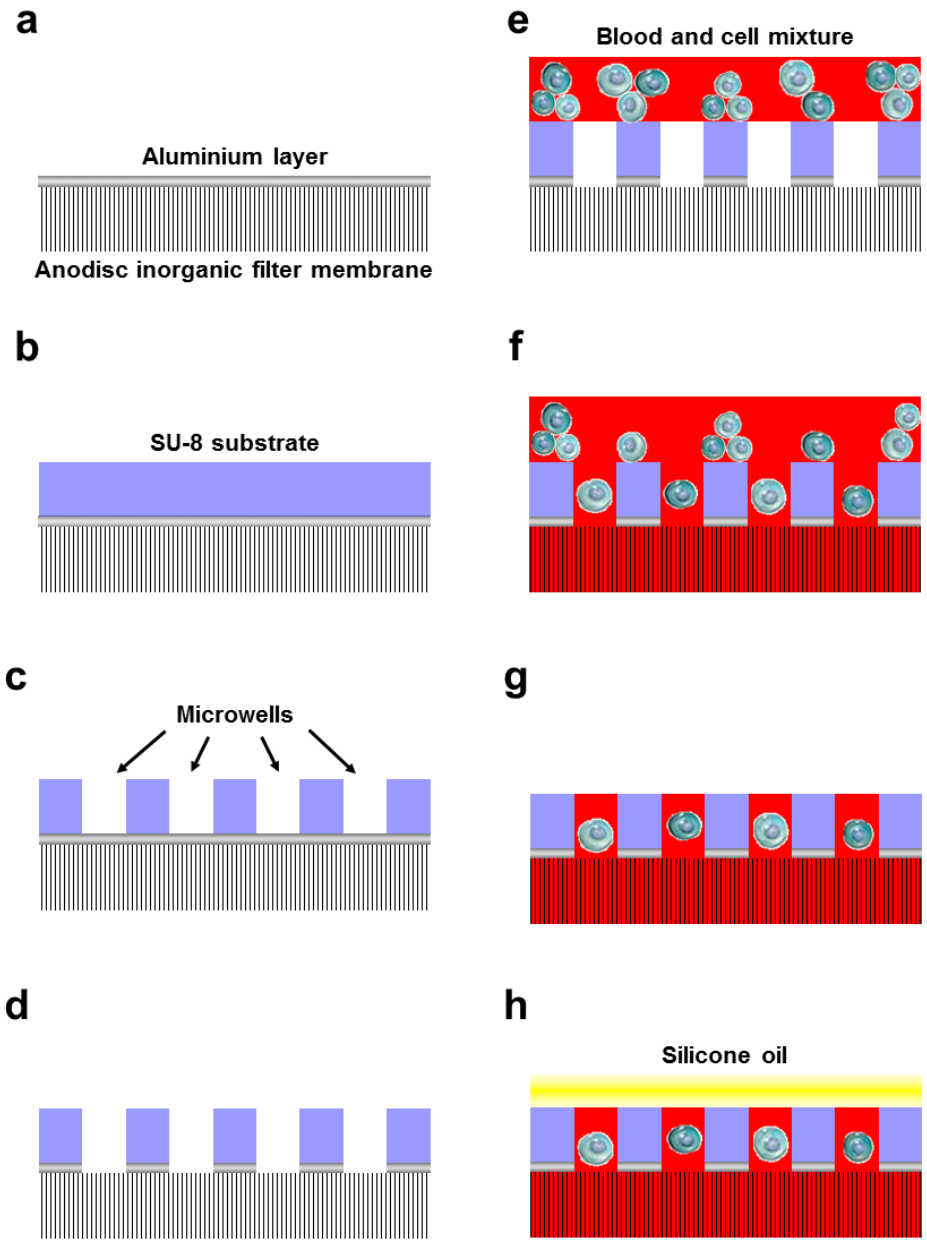

Supplementary Figure 2. Fabrication and operation of the high-density microwell array. a-d, Fabrication process of the high-density microwell array. a, A 400 nm thick layer of aluminium (gray) was deposited on one side of a 60 μm thick Anodisc inorganic filter membrane (black and white). b, A 50 μm layer of SU-8 (blue) was coated on top of the aluminium layer. c, Microwells

were developed in the SU-8 substrate. d, The aluminium layer beneath the microwells was etched away, while the remaining part of the aluminium layer was kept. e-h, Operation of the high-density microwell array. e, Single-cell suspension mixed with blood was spread on the surface of the microwell array. f, Blood-cell mixture settled in the microwells. The blood was able to enter the Anodisc while the target cells could only enter the microwells because of the size. g, The cells and blood outside the microwells were removed by flushing the microwell array with blood and fresh cell culture medium and drawing a small rubber squeegee across the flat surface. h, The microwell array was sealed by immersing it into silicone oil (yellow).

Supplementary Figure 3. Changes of single-cell OCRs in A549 human epithelial lung cancer cells with different metabolic inhibitors.

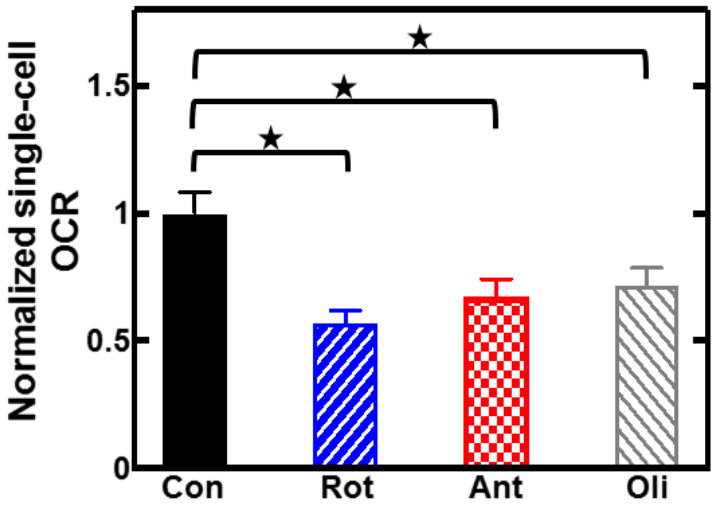

Supplementary Figure 3. Changes of single-cell OCRs in A549 human epithelial lung cancer cells with different metabolic inhibitors (n = 4 groups; 6743 cells; *p = 0.013, 0.018, 0.019; paired one-tailed t-tests were used in the statistical testing; error bars are s.e.). Con, control group; Rot, rotenone (2 μM); Ant, antimycin (2 μM); Oli, oligomycin (12 μM).

Supplementary Figure 4. Single-cell OCR distributions of normal and cancer cells from Patient 2 measured by SCM-PAM.

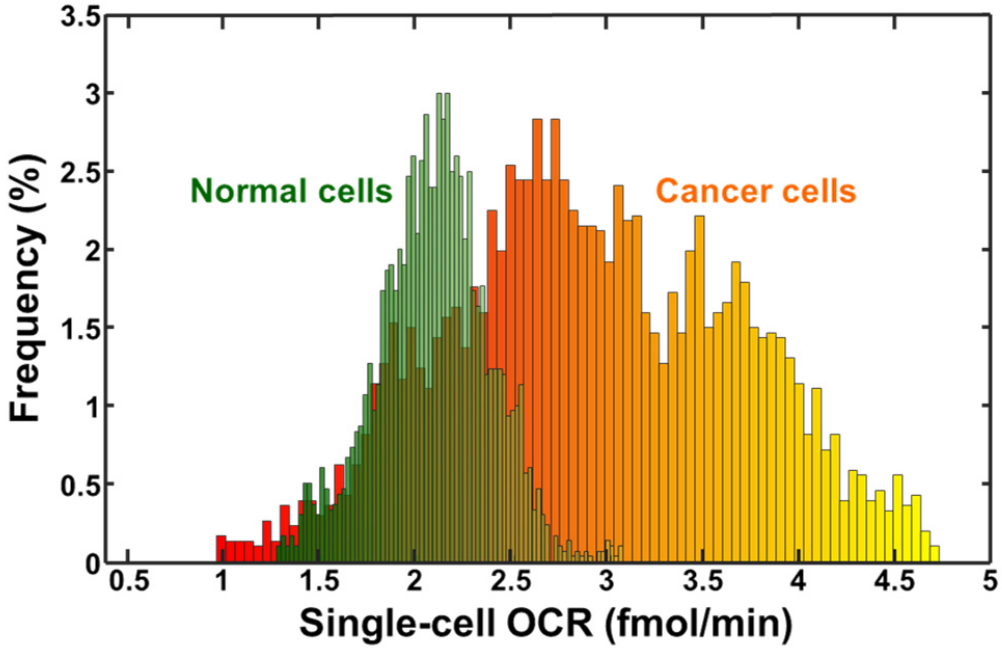

Supplementary Figure 4. Single-cell OCR distributions of normal and cancer cells from Patient 2 measured by SCM-PAM.

Supplementary Figure 5. Single-cell OCR distributions of normal and cancer cells from Patient 3 measured by SCM-PAM.

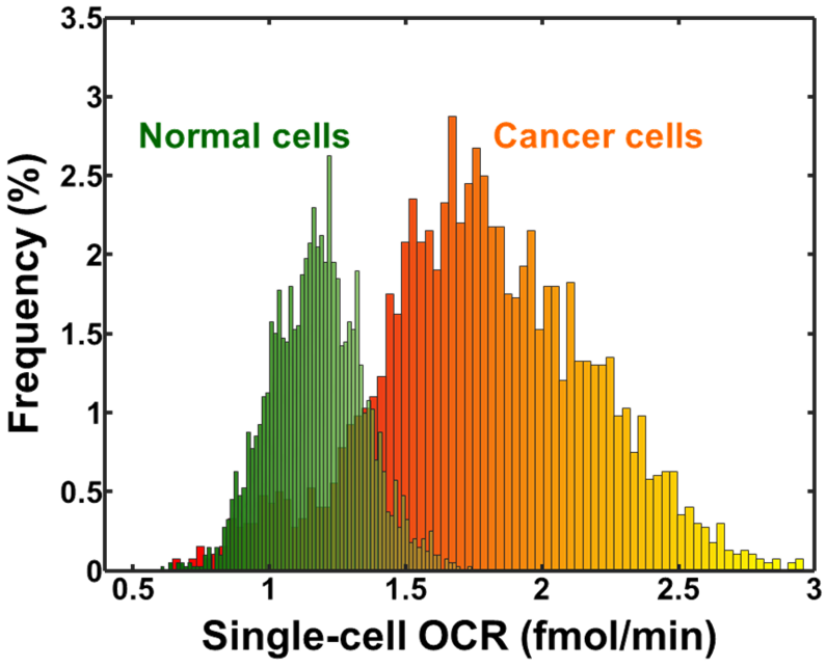

Supplementary Figure 5. Single-cell OCR distributions of normal and cancer cells from Patient 3 measured by SCM-PAM.

Supplementary Figure 6. Absolute changes in oxygen consumption of cancer and normal cells in hypoxia measured by SCM-PAM.

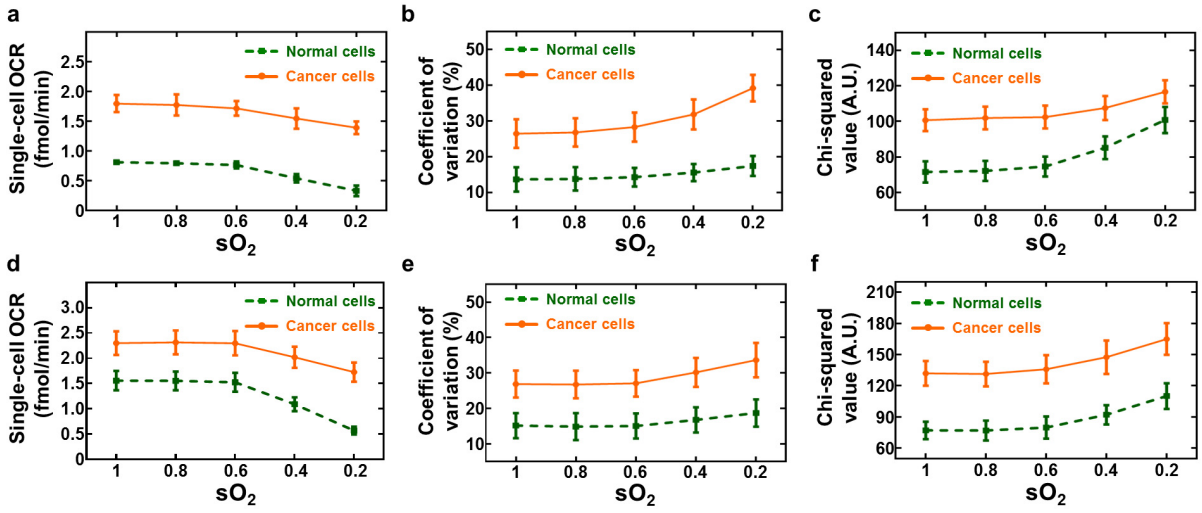

Supplementary Figure 6. Absolute changes in oxygen consumption of cancer and normal cells in hypoxia measured by SCM-PAM. a-c, Absolute changes in oxygen consumption of cultured cells in hypoxia measured by SCM-PAM. a, Average single-cell OCRs of cultured normal (RAW264.7 murine macrophage) and cancer (A549 human epithelial lung cancer) cells at different sO_2 levels (n = 5 groups, error bars are s.d.). b, CoVs of single-cell OCR distributions in cultured normal and cancer cells at different sO_2 levels (n = 5 groups, error bars are s.d.). c, Chi-squared values of single-cell OCR distributions in cultured normal and cancer cells at different sO_2 levels (n = 5 groups, error bars are s.d.). d-f, Absolute changes in oxygen consumption of normal and cancer cells from breast cancer patients in hypoxia measured by SCM-PAM. d, Average single-cell OCRs of normal and cancer cells from breast cancer patients at different sO_2 levels (n = 3 patients, error bars are s.d.). e, CoVs of single-cell OCR distributions in normal and cancer cells from breast cancer patients at different sO_2 levels (n = 3

patients, error bars are s.d.). f, Chi-squared values of single-cell OCR distributions in normal and cancer cells from breast cancer patients at different sO_2 levels (n = 3 patients, error bars are s.d.).

Supplementary Figure 7. Variation of the total haemoglobin content in a microwell with blood only or with blood-cell mixture.

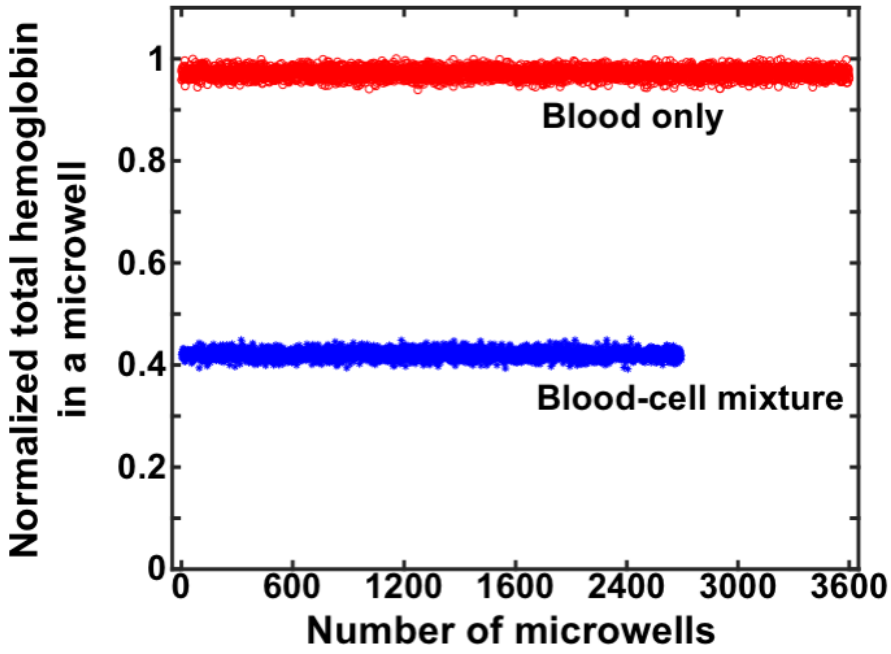

Supplementary Figure 7. Variation of the total haemoglobin content in a microwell with blood only or with blood-cell mixture. The total haemoglobin in each microwell was normalized to the well with the most haemoglobin.

Supplementary Figure 8. Fitting of single-cell OCR distributions of cancer cells to the sum of multiple normal distributions.

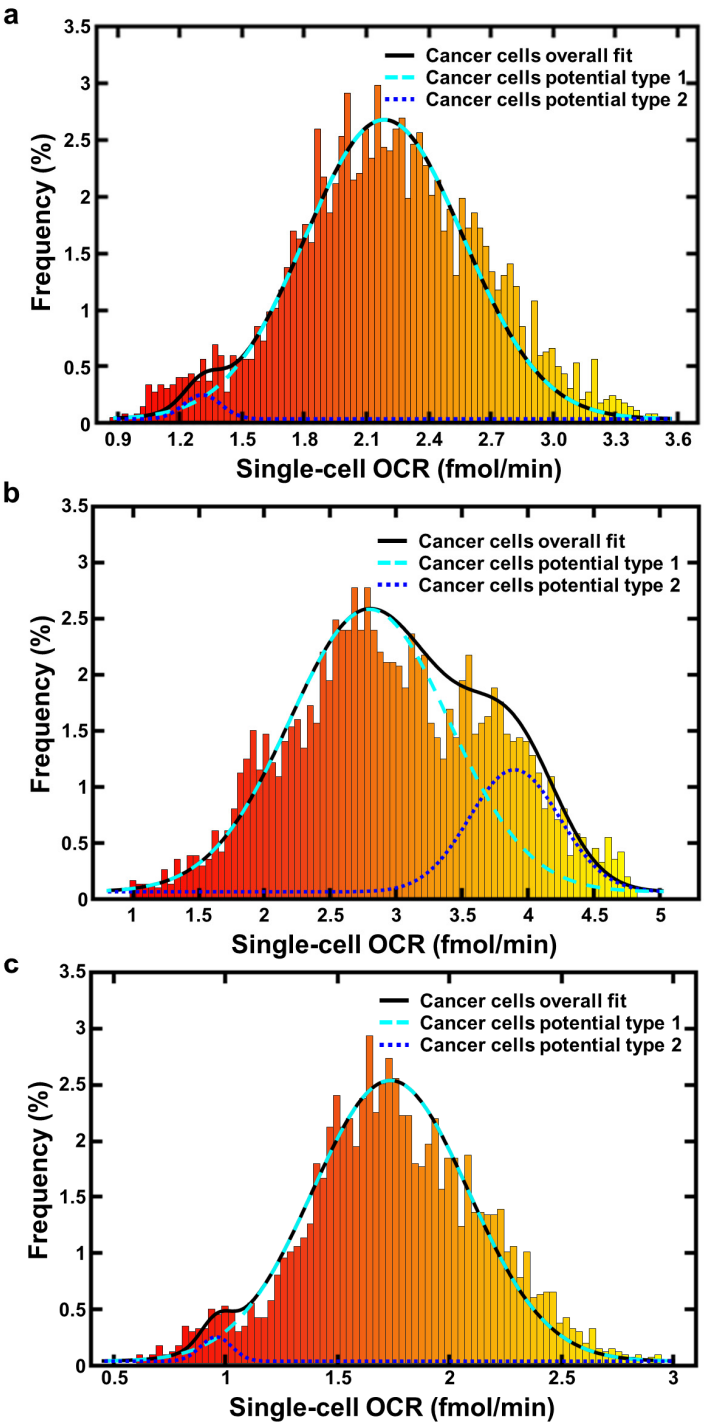

Supplementary Figure 8. Fitting of single-cell OCR distributions of cancer cells to the sum of multiple normal distributions. a, The single-cell OCR distribution of cancer cells in Patient 1 was fitted to the sum of two normal distribution with an R^2 value of 0.92, indicating that there may be two major types of cancer cells (indicated by the cyan dashed line and blue dotted line) within the cell population examined. b, The single-cell OCR distribution of cancer cells in Patient 2 was fitted to the sum of two normal distribution with an R^2 value of 0.84, indicating that there may be two major types of cancer cells (indicated by the cyan dashed line and blue dotted line) within the cell population examined. c, The single-cell OCR distribution of cancer cells in Patient 3 was fitted to the sum of two normal distribution with an R^2 value of 0.88, indicating that there may be two major types of cancer cells (indicated by the cyan dashed line and blue dotted line) within the cell population examined.